ARMY RESEARCH LABORATORY

The Strength of Binary Junctions in Hexagonal Close-Packed Crystals

by C.-C. Wu, P. W. Chung, S. Aubry, L. B. Munday, and A. Arsenlis

ARL-RP-477 **March 2014**

A reprint from *Acta Materialia*, Vol. 61, pp. 3422–3431, 2013.

NOTICES

Disclaimers

The findings in this report are not to be construed as an official Department of the Army position unless so designated by other authorized documents.

Citation of manufacturer's or trade names does not constitute an official endorsement or approval of the use thereof.

Destroy this report when it is no longer needed. Do not return it to the originator.

Army Research Laboratory
Aberdeen Proving Ground, MD 21005-5067

ARL-RP-477 **March 2014**

The Strength of Binary Junctions in Hexagonal Close-Packed Crystals

C.-C. Wu
Oak Ridge Affiliated Universities

P. W. Chung and L. B. Munday
Computational and Information Sciences Directorate, ARL

S. Aubry and A. Arsenlis
Lawrence Livermore National Laboratory

A reprint from *Acta Materialia*, Vol. 61, pp. 3422–3431, 2013.

REPORT DOCUMENTATION PAGE

Form Approved
OMB No. 0704-0188

1. REPORT DATE *(DD-MM-YYYY)*	2. REPORT TYPE	3. DATES COVERED (From - To)
March 2014	Reprint	1 August 2012–31 August 2013

4. TITLE AND SUBTITLE
The Strength of Binary Junctions in Hexagonal Close-Packed Crystals

5a. CONTRACT NUMBER

5b. GRANT NUMBER

5c. PROGRAM ELEMENT NUMBER

6. AUTHOR(S)
C.-C. Wu,[*] P. W. Chung, S. Aubry,[†] L. B. Munday, and A. Arsenlis[†]

5d. PROJECT NUMBER

5e. TASK NUMBER

5f. WORK UNIT NUMBER

7. PERFORMING ORGANIZATION NAME(S) AND ADDRESS(ES)
U.S. Army Research Laboratory
ATTN: RDRL-CIH-C
Aberdeen Proving Ground, MD 21005-5067

8. PERFORMING ORGANIZATION REPORT NUMBER
ARL-RP-477

9. SPONSORING/MONITORING AGENCY NAME(S) AND ADDRESS(ES)

10. SPONSOR/MONITOR'S ACRONYM(S)

11. SPONSOR/MONITOR'S REPORT NUMBER(S)

12. DISTRIBUTION/AVAILABILITY STATEMENT
Approved for public release; distribution is unlimited.

13. SUPPLEMENTARY NOTES
A reprint from *Acta Materialia*, Vol. 61, pp. 3422–3431, 2013.
[*]Oak Ridge Affiliated Universities, 4692 Millennium Drive, Ste. 101, Belcamp, MD 21017
[†]Lawrence Livermore National Laboratory, Livermore, CA 94551-0808

A comparative study of non-coplanar binary dislocation junctions in magnesium (Mg) and beryllium (Be) is presented to examine the effects of elastic properties and active Burgers vectors on junction formation and destruction in hexagonal close-packed (hcp) crystals via discrete dislocation dynamics simulations. Two junction configurations formed at intersecting prismatic $(01\bar{1}0)$/basal (0001) planes and type-II pyramidal $(\bar{2}112)$/prismatic $(01\bar{1}0)$ planes are studied using Burgers vectors of varying magnitudes. The equilibrium junctions are created from two intersecting straight gliding dislocations, and their subsequent strengths are evaluated under uniform applied stresses. The relative junction strengths between Mg and Be are consistent with their relative elastic stiffness, i.e., the modulus of elasticity for Mg is approximately one order of magnitude smaller than that of Be, and their junction strengths are similarly one order of magnitude apart. In general, the yield surfaces for junctions in Be are larger than those in Mg after normalization with the respective elastic moduli and Poisson's ratios. All yield surfaces exhibit a strong symmetry. However, the size and shape of the yield surfaces depend on the slip systems, especially the active Burgers vectors. The yield surfaces of hcp crystals can resemble those of face-centered cubic or body-centered cubic crystals when the active Burgers vectors of the dislocations involved in the junction are of type $\langle a\rangle$, namely $\frac{1}{3}\langle 11\bar{2}0\rangle$, and are distinct when Burgers vectors of different types are used: for instance, a type $\langle a+c\rangle$, namely $\frac{1}{3}\langle 11\bar{2}\bar{3}\rangle$, interacting with a type $\langle a\rangle$. It was also found that junctions with more edge part exhibit more elongated yield surfaces than those with more screw part, and slip systems involved with $\langle a\rangle$ Burgers vectors result in smaller yield surfaces. These results demonstrate that junction strengths for hcp crystals are largely determined by elastic properties and Burgers vectors. The work aims to assess the effects of intrinsic material properties and dislocation slip systems on the strength of different binary dislocation junctions for general hcp structures.

15. SUBJECT TERMS
discrete dislocation dynamics, strength, yield surfaces, HCP metals

16. SECURITY CLASSIFICATION OF:			17. LIMITATION OF ABSTRACT	18. NUMBER OF PAGES	19a. NAME OF RESPONSIBLE PERSON
a. REPORT	b. ABSTRACT	c. THIS PAGE			C.-C. Wu
Unclassified	Unclassified	Unclassified	UU	16	19b. TELEPHONE NUMBER (*Include area code*) 410-278-0985

Available online at www.sciencedirect.com

SciVerse ScienceDirect

Acta Materialia 61 (2013) 3422–3431

Acta MATERIALIA

www.elsevier.com/locate/actamat

The strength of binary junctions in hexagonal close-packed crystals

C.-C. Wu [a,b,*], P.W. Chung [b], S. Aubry [c], L.B. Munday [b], A. Arsenlis [c]

[a] Oak Ridge Affiliated Universities Research Associate at the Computational and Information Sciences Directorate, US Army Research Laboratory, Aberdeen Proving Ground, MD 21005, USA

[b] Computational and Information Sciences Directorate, US Army Research Laboratory, Aberdeen Proving Ground, MD 21005, USA

[c] High Performance Computational Materials Science and Chemistry Group, Condensed Matter and Materials Division, Lawrence Livermore National Laboratory, PO Box 808, L-367 Livermore, CA 94551-0808, USA

Received 14 December 2012; accepted 19 February 2013
Available online 18 March 2013

Abstract

A comparative study of non-coplanar binary dislocation junctions in magnesium (Mg) and beryllium (Be) is presented to examine the effects of elastic properties and active Burgers vectors on junction formation and destruction in hexagonal close-packed (hcp) crystals via discrete dislocation dynamics simulations. Two junction configurations formed at intersecting prismatic $(0\,1\,\bar{1}\,0)$/basal $(0\,0\,0\,1)$ planes and type-II pyramidal $(\bar{2}\,1\,1\,2)$/prismatic $(0\,1\,\bar{1}\,0)$ planes are studied using Burgers vectors of varying magnitudes. The equilibrium junctions are created from two intersecting straight gliding dislocations, and their subsequent strengths are evaluated under uniform applied stresses. The relative junction strengths between Mg and Be are consistent with their relative elastic stiffness, i.e., the modulus of elasticity for Mg is approximately one order of magnitude smaller than that of Be, and their junction strengths are similarly one order of magnitude apart. In general, the yield surfaces for junctions in Be are larger than those in Mg after normalization with the respective elastic moduli and Poisson's ratios. All yield surfaces exhibit a strong symmetry. However, the size and shape of the yield surfaces depend on the slip systems, especially the active Burgers vectors. The yield surfaces of hcp crystals can resemble those of face-centered cubic or body-centered cubic crystals when the active Burgers vectors of the dislocations involved in the junction are of type $\langle a\rangle$, namely $\frac{1}{3}\langle 1\,1\,\bar{2}\,0\rangle$, and are distinct when Burgers vectors of different types are used: for instance, a type $\langle a+c\rangle$, namely $\frac{1}{3}\langle 1\,1\,\bar{2}\,\bar{3}\rangle$, interacting with a type $\langle a\rangle$. It was also found that junctions with more edge part exhibit more elongated yield surfaces than those with more screw part, and slip systems involved with $\langle a\rangle$ Burgers vectors result in smaller yield surfaces. These results demonstrate that junction strengths for hcp crystals are largely determined by elastic properties and Burgers vectors. The work aims to assess the effects of intrinsic material properties and dislocation slip systems on the strength of different binary dislocation junctions for general hcp structures.

Keywords: Discrete dislocation dynamics; Strength; Yield surface; hcp Metals

1. Introduction

Recent progress in the development of new lightweight structural materials and low-loss wide band-gap semiconductor materials has fostered great interest in dislocation mechanisms in hexagonal close-packed (hcp) crystals. The formability of hcp crystals such as Mg and Be and the deleterious electronic properties of threading dislocations in wide band-gap gallium nitride (a wurtzite crystal structure consisting of two interpenetrating hcp lattices) pose questions regarding dislocation properties and, in particular, the fundamental mechanisms that would enable "designability" of the dislocation content. Among the many issues potentially relevant to designability, entanglements of dislocations by way of binary junctions are of keen interest.

From general dislocation theory, two or more intersecting dislocations gliding on adjacent slip planes can attract each other and form junctions to reduce the total strain energy [1–3]. These junctions are usually sessile, with

* Corresponding author at: Computational and Information Sciences Directorate, US Army Research Laboratory, Aberdeen Proving Ground, MD 21005, USA. Tel.: +1 410 278 0985; fax: +1 410 278 4983.
E-mail address: chi-chin.wu.ctr@mail.mil (C.-C. Wu).

1359-6454/$36.00
http://dx.doi.org/10.1016/j.actamat.2013.02.033

locked dislocation arms that can act as obstacles and restrict the movements and interactions of other dislocations (such as the Lomer–Cottrell or Hirth lock). With a sufficiently high dislocation density, dislocations are more likely to intersect and form junctions as long as they are energetically favorable. Possible junction formation and dislocation interactions in a network are normally modeled with a glissile dislocation sweeping through a forest of equally spaced and parallel dislocations on another intersecting slip plane [4,5]. Significant efforts in studying the flow stress effect by this type of multi-junction interaction can be traced back to Shoeck and Frydman's work four decades ago [6]. Using an improved line tension model similar to the approach by Hirth [3], Shoeck and Frydman [6] first computed the interactions of a single binary junction due to dislocation intersection. The interactions were then expanded to approximate the overall blocking effect due to multiple junctions in the entire dislocation network, using an averaging procedure in order to take into account other possible interactions. The simplification of Shoeck and Frydman's model, which assumed an equal value for the tree length and the average separation distance in the forest, put the accuracy of Shoeck and Frydman's predictions into question [7]. In recent years, the quantitative relation between the flow stress describing the blocking effect and the dislocation density is generally known as analogous to that between the internal shear stress and the dislocation density in cold working [8]. The detailed mechanisms due to multi-junctions have also been studied via DDD simulations [9,10]. It has been shown that junctions can directly relate to the local dislocation microstructure and indirectly affect important properties such as the overall dislocation density, stress–strain response and yield strength [4,6]. Existing studies of binary junctions mostly seek the regimes where a junction can form using the initial orientations of intersecting dislocations as variables. For face-centered cubic (fcc) crystals, early work by Hirth [3] examined different binary junction strengths for all the combinations of possible pairs of dislocations. Hirth determined the junction strength relative to the maximum resolved shear stress via the calculated energy reduction due to junction formation. With a similar approach, Dupuy and Fivel [11] developed an improved line tension model, taking into account the contribution of forces due to the line tension perpendicular to the dislocation direction. Using this approach, they estimated the strengths of different junctions in fcc crystals. Simulation techniques such as molecular dynamics (MD) [7,12–14] and discrete dislocation dynamics (DDD) [10,15–23], which can reveal dynamical dislocation mechanisms, have also been employed to study dislocation junctions. For example, via MD simulations, Rodney and Phillips [14] compared the calculated critical stress to break the Lomer–Cottrell junction in a fcc crystal and identified a temporary length increase prior to unzipping when a binary junction is loaded by an increasing stress. This is a mechanism unexpected by the line tension approximation, which would have predicted a monotonically decreasing junction length. Most reported studies on strength only estimate the magnitudes of critical resolved stresses as the junction strength, such as Hirth's energy calculations [3] and Rodney and Phillips' MD simulations for fcc crystals [14]. To the best of the present authors' knowledge, a more quantitatively comprehensive illustration of junction strength was first shown by Shenoy et al. [19], where the junction strength of a symmetric Lomer–Cottrell lock in fcc crystals was described with a yield surface estimated by DDD simulations. Despite the fact that the yield surface was composed of individual points, it provided insight on the resistance of the lock to breaking as a result of the applied stresses. Via the yield surface, the strength of a junction can be estimated quantitatively by any loading condition of the applied stresses because the stable region of a junction is contained by a closed envelope.

Dislocation junctions have been studied previously, either for their formation or for their strength (destruction) properties. As the prior references illustrate, most efforts have focused on cubic crystals, especially fcc metals. This is partly because most structural materials fall into this category where only one unique dislocation slip system needs to be considered because of their high crystallographic symmetry. In contrast, there are several possible slip systems for dislocations in hcp crystals, because of their lower crystallographic symmetry. Furthermore, only a few researchers have studied non-coplanar binary junctions in hcp [22–24]. In hcp crystals particularly, dislocations can glide from a primary plane to an adjacent secondary plane, because a junction can serve as a dislocation source for cross slip [24]. Therefore, the presence of junctions can have a significant effect on important macroscopic properties. Junction strength may also play a role in dislocation mechanisms near grain boundaries [25,26]. In wurtzite crystals, experimental findings have indicated that the global dislocation density is closely correlated with the annihilation and entanglement of threading dislocations, both of which are mechanisms that are critically related to junction strength [27–29].

Nevertheless, studies of junction strengths for hcp crystals are scarcer, and it is unclear to what degree knowledge of fcc crystals is applicable because of the greater complexity of crystal structure and, more importantly, multiple possible dislocation slip systems. Using a DDD approach, Capolungo [22] compared the strengths of binary junctions formed at the intersections of primary slip planes, including basal, prismatic and pyramidal planes. Given that the dislocation mobility may vary from one slip system to another and to date has not been well documented for hcp crystals, Capolungo [22] used the mobility law that Monnet et al. [23] had approximated for dislocations on prismatic slip planes for zirconium (Zr). However, the choice of mobility should not play an important role in determining the resultant junction strengths because of the insensitivity of the yield stress to substantial changes in mobility observed by Monnet et al. [23].

In the present work, DDD simulations are employed to study the strength of binary junctions formed by two non-coplanar dislocations in Mg and Be crystals. Their different elastic constants and c/a ratios (where the c and a represent the vertical and lateral lattice spacings in hcp crystals, respectively) make them useful for detecting similarities and differences in binary junctions in general hcp crystals [30]. Two junction configurations formed at the intersecting edges of the same prismatic $(0\,1\,\bar{1}\,0)$ plane with the basal $(0\,0\,0\,1)$ and with the type-II pyramidal $(\bar{2}\,1\,1\,2)$ planes are studied. The type II-pyramidal plane is chosen in particular because of its importance as a slip plane in several hcp and hcp-related structures, such as wurtzite crystals [31,32]. A variety of Burgers vector pairs are employed to examine their effects on junction strengths. Burgers vectors are henceforth defined as $\frac{1}{3}\langle 1\,1\,\bar{2}\,0\rangle$ for pure $\langle a\rangle$ type, $\langle 0\,0\,0\,1\rangle$ for pure $\langle c\rangle$ type, and $\frac{1}{3}\langle 1\,1\,\bar{2}\,\bar{3}\rangle$ for $\langle a+c\rangle$ type, where a and c refer to the lattice spacings in the basal plane and its normal directions, respectively. The paper is organized as follows. Section 2 presents the calculation methodology along with the problem setup and assumptions. The results are presented in Section 3, with extensive discussions of the observations, focusing on how the differences in the elastic constants and the Burgers vectors affect junction strengths in terms of the sizes and shapes for the yield surfaces. Finally, the paper ends with conclusions in Section 4.

2. Methodology

The dislocation dynamics simulator ParaDiS [33] was employ in this work. To remain consistent with the implementation of hexagonal Miller indices in ParaDiS, the three index convention is used henceforth to represent directions and planes, with the understanding that the conventional 4-index notation for hexagonal axes can be readily converted [34]. The calculations are performed in two steps. The first step establishes the equilibrium unstressed junction via equilibration simulations. Then, in the second step, stress is applied to the junction so as to result in unzipping, i.e., complete destruction or dissociation of the junction.

Despite their known anisotropic properties, both Be and Mg are approximated to be isotropic to first order in their dislocation junction behaviors: Be is known to be the least anisotropic metal among all hcp single crystals, and Mg also does not significantly deviate from isotropic linear elasticity, given the ratio between the two elastic constants C_{66}:C_{44} is close to 1 (1.030) [30,35]. Capolungo [36] also studied the effects of elastic anisotropy and suggested the suitability of using isotropy to approximate long-range dislocation interactions in Mg.

The equilibrium non-coplanar junctions are first formed by inserting into the center of a three-dimensional simulation box two straight dislocation lines $\boldsymbol{\xi}_1$ and $\boldsymbol{\xi}_2$, each of length $40{,}000a$, where a is the lattice spacing in the basal plane. The sets of interacting slip systems are specified in Table 1 and schematically illustrated in Fig. 1. Table 2 lists the Burgers vectors and directions for the resultant junctions. The Burgers vectors are chosen such that interaction leads to the formation of a junction along the direction parallel to the intersecting edge of the adjacent slip planes. For the basal/prismatic junction in case (a), the $\langle a\rangle$-type Burgers vectors for the intersecting dislocations result in a junction also with an $\langle a\rangle$-type Burgers vector. For the type-II pyramidal/prismatic junction, the $\langle a+c\rangle$-type Burgers vector is used for the pyramidal plane and both $\langle a\rangle$ and $\langle c\rangle$-types are considered for the prismatic plane. Therefore, cases (b) and (c) refer to the same junction formed on the intersecting planes using different pairs of Burgers vectors. An $\langle a+c\rangle$-type Burgers vector for the prismatic plane is not considered here because a $\langle 2a\rangle$-type junction has a larger energy than two $\langle a\rangle$-type junctions. Nor are junction results shown for dislocation pairs involving an $\langle a\rangle$-type and a $\langle c\rangle$-type Burgers vector, because junction formation is not favorable in that scenario. Pairs using pure $\langle c\rangle$-type Burgers vectors also do not form a junction. Both the 4-index notation commonly used for hcp crystals and the equivalent 3-index notation are listed in Table 1. The isotropic elastic constants used for Be and Mg are listed in Table 3 [35]. The magnitudes of the Burger vectors in the lateral and vertical directions and can therefore be calculated by the specified lattice spacing and the c/a ratio.

Table 1
hcp Slip planes and Burgers vectors studied in this work.

	Slip plane		Burgers vector		
	4-index	3-index	4-index	3-index	Type
(a)	$(0\,0\,0\,1)$	$(0\;0\;\frac{c}{a})$	$\frac{1}{3}[1\,\bar{2}\,1\,0]$	$\left[\frac{1}{2}\;\frac{\sqrt{3}}{2}\;0\right]$	$\langle a\rangle$
	$(0\,1\,\bar{1}\,0)$	$(\sqrt{3}\;1\;0)$	$\frac{1}{3}[\bar{2}\,1\,1\,0]$	$\left[\frac{1}{2}\;-\frac{\sqrt{3}}{2}\;0\right]$	$\langle a\rangle$
(b)	$(\bar{2}\,1\,1\,2)$	$(-\sqrt{3}c\;3c-2\sqrt{3}a)$	$\frac{1}{3}[2\,\bar{1}\,\bar{1}\,3]$	$\left[-\frac{1}{2}\;\frac{\sqrt{3}}{2}\;\frac{c}{a}\right]$	$\langle a+c\rangle$
	$(0\,1\,\bar{1}\,0)$	$(\sqrt{3}\;1\;0)$	$\frac{1}{3}[\bar{2}\,1\,1\,0]$	$\left[\frac{1}{2}\;-\frac{\sqrt{3}}{2}\;0\right]$	$\langle a\rangle$
(c)	$(\bar{2}\,1\,1\,2)$	$(-\sqrt{3}c\;3c-2\sqrt{3}a)$	$\frac{1}{3}[2\,\bar{1}\,\bar{1}\,3]$	$\left[-\frac{1}{2}\;\frac{\sqrt{3}}{2}\;\frac{c}{a}\right]$	$\langle a+c\rangle$
	$(0\,1\,\bar{1}\,0)$	$(\sqrt{3}\;1\;0)$	$[0\,0\,0\,\bar{1}]$	$\left[0\;0\;-\frac{c}{a}\right]$	$\langle c\rangle$

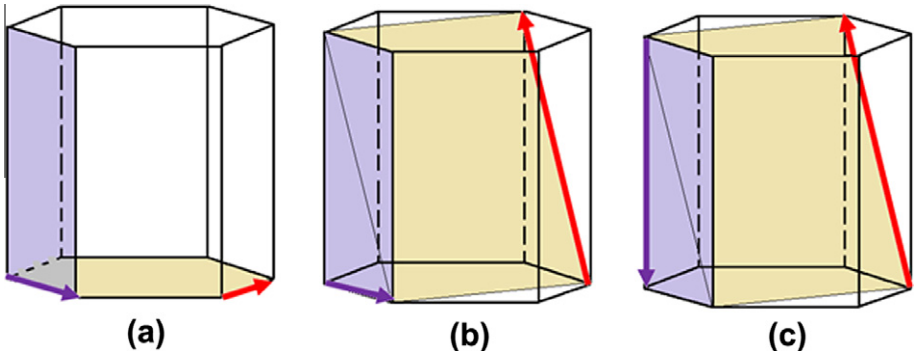

Fig. 1. Illustration showing the different interacting slip systems used in this work: The purple arrows represent the Burgers vectors for the dislocation on the $(01\bar{1}0)$ prismatic plane (also in purple). The red arrows represent the Burgers vectors for the dislocation on the basal plane (0001) in case (a) and on the type-II pyramidal plane $(\bar{2}112)$ in cases (b) and (c), respectively. (For interpretation of the references to colour in this figure legend, the reader is referred to the web version of this article.)

Table 2
Burgers vectors and directions of the resultant binary junctions.

	Burgers vector		Junction direction	
	4-Index	3-Index	4-Index	3-Index
(a)	$\frac{1}{3}[\bar{1}\bar{1}20]$	$[1\ 0\ 0]$	$[\bar{2}110]$	$[1\ -\sqrt{3}\ 0]$
(b)	$[0001]$	$[00\frac{c}{a}]$	$[2\bar{1}\bar{1}3]$	$[-1\sqrt{3}\ 2\frac{c}{a}]$
(c)	$\frac{1}{3}[2\bar{1}\bar{1}0]$	$[-\frac{1}{2}\ \frac{\sqrt{3}}{2}\ 0]$		

Table 3
Elastic constants for Be and Mg.

Property	Be	Mg
Modulus of elasticity μ (GPa)	130	17
Poisson's ratio v	0.032	0.290
Lattice spacing a (nm)	0.229	0.269
c/a ratio	1.568	1.633

The core radius of a dislocation is taken to be equivalent to the lattice spacing a, and the core energy was approximated by

$$E_c = \frac{\mu a^2}{4\pi} \ln\left(\frac{r_o}{0.1a}\right) \quad (1)$$

where E_c is the core energy (J m^{-1}), μ is the modulus of elasticity (Pa), r_o is the core radius, approximated as $1a$. The cubic simulation box is $600{,}000a$ on each side, and all dislocations are initially discretized into segments ranging in length from $1000a$ to $3000a$.

A series of test calculations are first performed [37] to find stable equilibrium junctions and thereby the most favorable initial orientations for the two intersecting dislocations. Fig. 2 schematically illustrates the dislocation configurations before and after the junction formation, with ψ_1 and ψ_2 and ψ_1' and ψ_2' indicating the angles that the intersecting dislocations $\boldsymbol{\xi}_1$ and $\boldsymbol{\xi}_2$ make with the junction direction before and after junction formation, respectively. Various junctions are tested to find the configuration with the lowest energy. The junctions are obtained by varying ψ_1 and ψ_2 in 30° intervals from −180° to +180° to generate 169 total initial intersections. From these, it was found that junctions can be formed in the absence of a net stress field when $\psi_1 = \psi_2 = 30°$ for the chosen slip systems. Then, a more refined calculation is performed to create the initial junctions. $\boldsymbol{\xi}_1$ and $\boldsymbol{\xi}_2$ are placed on their respective planes with their midpoints intersecting at O at angles $\psi_1 = \psi_2 = 30°$ to the prospective junction axis. The configuration is then allowed to evolve freely and self-equilibrate with a zero net stress field. The results are largely insensitive to dislocation length, i.e., the dislocations are effectively infinite in length, which was determined by comparing the results with those produced using virtual segments at the pinned end nodes. The relaxation is permitted to occur for 30,000 total time steps. The equilibrium junction length can be reached typically within 10,000 time steps. The equilibrium junction configuration is also indicated when the displacement of all nodes within a single

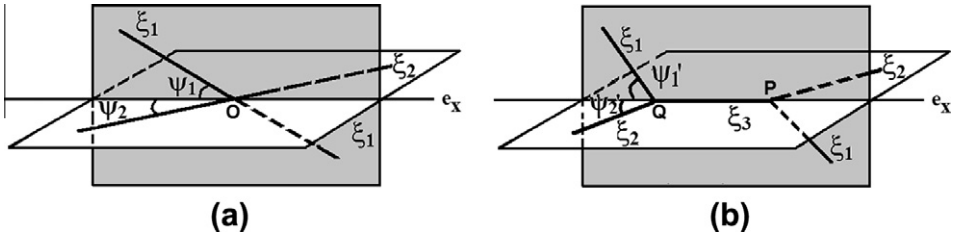

Fig. 2. Illustration showing dislocation configurations: (a) $\boldsymbol{\xi}_1$ gliding on plane 1 (gray) intersects with $\boldsymbol{\xi}_2$ gliding on plane 2 (white) at their midpoints O with both angles ψ_1 and ψ_2 30° to $\boldsymbol{e}_x$; (b) a junction $\boldsymbol{\xi}_3$ is formed along $\boldsymbol{e}_x$ and connected to $\boldsymbol{\xi}_1$ and $\boldsymbol{\xi}_2$ with triple nodes P and Q. After junction formation, the angles change to ψ_1' and ψ_2' for $\boldsymbol{\xi}_1$ and $\boldsymbol{\xi}_2$, respectively.

time step is sufficiently small (in the range 1×10^{-4} to $1 \times 10^{-3}a$). Dislocations are also confined on their slip planes via a constraint that, over a single time step, prevents each node from having a displacement component normal to its glide plane.

Depending on the magnitude and the direction of resolved stresses on the slip planes, dislocation junctions may be destabilized by an externally applied stress field. When the junction is unzipped along a straight line and dislocation arms are forbidden to climb, the dissolution of a junction is essentially carried out via the Frank–Read bow out mechanism of the arms induced by the resolved stress τ_o and can be approximated as [11,40–42]

$$\tau_o = \frac{\alpha \mu b}{l} \ln l \tag{2}$$

where α is a constant in the range 1.0–2.0, comprising the pre-logarithm term associated with the Poisson's ratio, v, used for the energy of dislocation line tension, b is the magnitude of Burgers vector, μ is the shear modulus, and l is the length of pinned straight dislocation segment prior to bowing out. Therefore, the critical resolved stress to break a junction is closely related to τ_o.

Upon equilibration of the junction, trial stresses $\boldsymbol{\sigma}$ are applied until "unzipping" of the junction is observed, thereby determining the junction strength. In principle, the relation between the applied stress field $\boldsymbol{\sigma}$ and the resolved shear stress on each dislocation σ_i ($i = 1$, 2 and 3, corresponding to dislocations $\boldsymbol{\xi}_1$, $\boldsymbol{\xi}_2$ and $\boldsymbol{\xi}_3$, respectively), should be

$$\begin{aligned} \sigma_1 &= \boldsymbol{\sigma} : \boldsymbol{s}_1 \\ \sigma_2 &= \boldsymbol{\sigma} : \boldsymbol{s}_2 \\ \sigma_3 &= \boldsymbol{\sigma} : \boldsymbol{s}_3 \end{aligned} \tag{3}$$

where $\boldsymbol{\sigma}$ is the applied 3×3 stress tensor, and $\boldsymbol{s}_i$ are the 3×3 projection matrices, which can be calculated from the Burgers vector $\boldsymbol{b}_i$ and the unit normal vector $\boldsymbol{n}_i$ ($i = 1, 2, 3$) for each dislocation, including the two interacting dislocations ($i = 1, 2$) and the resultant junction ($i = 3$), as

$$\boldsymbol{s}_i = \left(\frac{\boldsymbol{b}_i}{|\boldsymbol{b}_i|} \otimes \frac{\boldsymbol{n}_i}{|\boldsymbol{n}_i|} + \frac{\boldsymbol{n}_i}{|\boldsymbol{n}_i|} \otimes \frac{\boldsymbol{b}_i}{|\boldsymbol{b}_i|} \right) \tag{4}$$

To ensure that the stress on one plane does not cause a resolved shear on the other, an additional constraint is applied, using the orthogonal Schmidt tensors $\boldsymbol{S}$, such that for $j, k = (1, 2, 3)$ [38,39]

$$\boldsymbol{S}_j := \boldsymbol{s}_k = \boldsymbol{\delta}_{jk} \tag{5}$$

where $\boldsymbol{\delta}_{jk}$ is one when $j = k$, and zero otherwise. The resolved shear stress σ_i on each dislocation can then be calculated as

$$\begin{aligned} \sigma_1 &= \boldsymbol{\sigma} : \boldsymbol{S}_1 \\ \sigma_2 &= \boldsymbol{\sigma} : \boldsymbol{S}_2 \\ \sigma_3 &= \boldsymbol{\sigma} : \boldsymbol{S}_3 \end{aligned} \tag{6}$$

where now σ_1, σ_2 and σ_3 are independent of each other. That is, the applied stress $\boldsymbol{\sigma}$ for breaking the junction can be calculated as

$$\boldsymbol{\sigma} = \sigma_1 \boldsymbol{S}_1 + \sigma_2 \boldsymbol{S}_2 + \sigma_3 \boldsymbol{S}_3 \tag{7}$$

The σ_3 is set to zero in this work, preventing the junction from bowing out on either slip plane. Therefore, the trial applied stress $\boldsymbol{\sigma}$ only depends on the resolved stresses σ_1 and σ_2 on dislocations $\boldsymbol{\xi}_1$ and $\boldsymbol{\xi}_2$, respectively, and Eq. (6) becomes

$$\boldsymbol{\sigma} = \sigma_1 \boldsymbol{S}_1 + \sigma_2 \boldsymbol{S}_2 \tag{8}$$

In the following, σ_2 refers to the resolved stress on the prismatic plane $(01\bar{1}0)$, and σ_1 corresponds to the stress applied on the basal plane (0001) for case (a) and the type-II pyramidal plane $(\bar{2}112)$ for cases (b) and (c). For each specified ratio of σ_1/σ_2, the equilibrium junction is loaded with the stress tensor $\boldsymbol{\sigma}$, starting with the smallest magnitude. If the junction remains after 30,000 total time steps, the stress is incrementally increased and the equilibration is repeated. The critical values of the stress pair (σ_{1c}, σ_{2c}) are recorded when destruction or dissolution is observed. In this work, that point is reached if either of the following conditions is met: the dislocations completely detach; or the junction length becomes nil. Upon scaling with a normalization factor, the locus of points defined by (σ_{1c}, σ_{2c}) constitutes the yield surface of the junction.

3. Results and discussion

3.1. The formation of equilibrium dislocation junctions

The initial equilibrium junction lengths and orientations of the dislocation arms are listed in Table 4. In this table, L_e is the equilibrium junction length in the unit of lattice spacing a, ΔE is the total energy reduction in percent due to junction formation, ψ_1' is the orientation of dislocation arms on the basal plane for case (a) and on the type-II pyramidal plane for cases (b) and (c), respectively, and ψ_2' is the dislocation arm orientation on the prismatic plane for all cases. Here, the angles are measured from the intersection edge of two slip planes to the dislocation arm, and ΔE is approximated based on the proportional relation between the energy of a dislocation and the magnitude of the Burgers vector. When the junction starts to form, it will

Table 4
Properties of the equilibrium junctions.

Case	Material	L_e (a)	ΔE (%)	ψ_1'/ψ_2'
(a)	Be	23,323	50	60°/60°
	Mg	23,769	50	62°/62°
(b)	Be	21,698	45	54°/65°
	Mg	16,145	43	45°/64°
(c)	Be	31,311	83	88°/75°
	Mg	26,029	84	78°/60°

continue growing until all forces at the triple nodes are balanced. These forces are the pulling forces due to the self-force and the dislocation interaction forces between each dislocation segment.

The results indicate that it is most energetically favorable to form the type-II pyramidal/prismatic junction with the $\langle a+c\rangle$-type Burgers vector on the pyramidal plane interacting with the $\langle c\rangle$-type Burgers vector on the prismatic plane, as shown in case (c). This junction has the largest equilibrium length among those tested. At equilibrium, on either slip plane, the dislocation on that plane intersects both triple points at the same angle with the junction line, regardless of the slip plane pairing. For both Be and Mg, the dislocation arms make identical angles, namely $\psi_1' = \psi_2'$, when the Burgers vectors of the two intersecting dislocations are the same—both are $\langle a\rangle$ type. However, choosing different magnitudes of Burgers vector yields different angles ($\psi_1' \neq \psi_2'$). As shown in Table 4, the junction configurations are associated with an identical prismatic plane, but intersecting with different adjacent planes—the basal plane for case (a) and the type II-pyramidal plane for cases (b) and (c). Via analytical calculations, Yoo et al. [24] predicted that the screw dislocations gliding on the type II-pyramidal plane have a greater difference in line tension between Be and Mg than those gliding on the basal plane. This is consistent with the finding of a greater difference in the equilibrium junction lengths between Be and Mg in case (b) than in case (a). The equilibrium length and arm orientations of the type-II pyramidal/prismatic junction are only sensitive to the choice of Burgers vector on the prismatic plane.

Distinctly different zipping mechanisms are also observed for the different Burgers vector pairs. In cases (a) and (b), where an $\langle a\rangle$-type Burgers vector is used for the dislocation on the prismatic plane, a zipping mechanism is observed similar to the formation mechanism seen in fcc and body-centered cubic crystals (e.g., Refs. [11,15]) often described as the movement of triple nodes in opposite directions along a straight line. This mechanism is depicted in Fig. 3a. In case (c), a Burgers vector associated with $\langle c\rangle$ is used for the dislocation on the prismatic plane. The intersecting dislocation arms rotate and approach each other such that they become nearly parallel to the junction direction, forming very shallow angles to the junction line, until they eventually combine to form the junction. Fig. 3b illustrates the junction formation for case (c) via this mechanism. In Fig. 3b, early, almost immediate, adjustment of line orientation for the dislocations near the intersection point appears. This is for two reasons. First, as indicated in Table 1, the two intersecting dislocations are predominantly screw-like. Secondly, the Burgers vector for the dislocation on the pyramidal plane is at the same direction as the junction axis $\boldsymbol{e_x}$, as depicted in Fig. 1b. Therefore, it is energetically favorable for this dislocation to orient parallel to $\boldsymbol{e_x}$. Furthermore, through the analytical calculation based on the Kroupa formula [43], it was found that, at the original intersecting orientation (i.e., $\psi_1 = \psi_2 = 30°$), a repulsive interaction exists between the two intersecting dislocations. However, the interaction becomes attractive after dislocation rotation and realignment due to a torque force. For Mg, some experimental findings suggest a "self-blocking" effect of the $\langle c+a\rangle$ dislocations on type

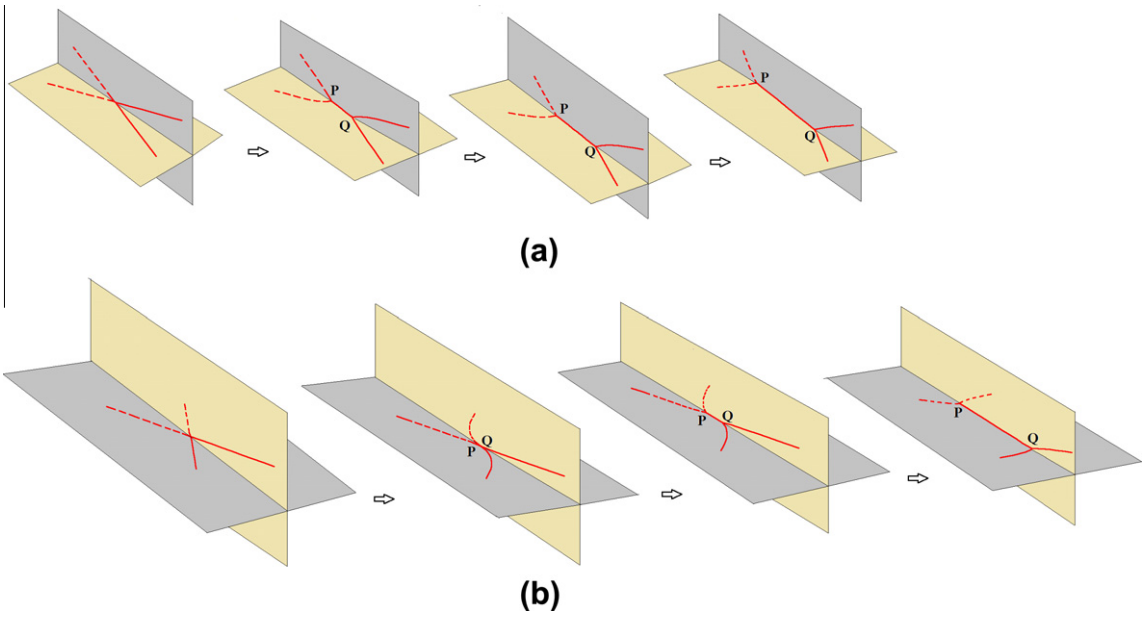

Fig. 3. Different mechanisms to form the junction: In (a) for case (a), the junction starts to form from the intersection and zip up progressively in opposite directions along the junction. In (b) for case (c), the dislocation arms on either side of the intersection rotate and align themselves parallel to the plane intersection until they eventually merge and form the junction. The gray plane represents the prismatic plane. The yellow plane corresponds to the basal plane in (a) and type II-pyramidal plane in (b). P and Q indicate the junction triple nodes. The junction in (a) is oriented along $[1\ -\sqrt{3}\ 0]$, equivalent to $[\bar{2}\,1\,1\,0]$ in the 4-index notation. The junction in (b) is oriented along $[-1\ \sqrt{3}\ 2\frac{c}{a}]$, equivalent to $[2\,\bar{1}\,\bar{1}\,3]$ in the 4-index notation. (For interpretation of the references to colour in this figure legend, the reader is referred to the web version of this article.)

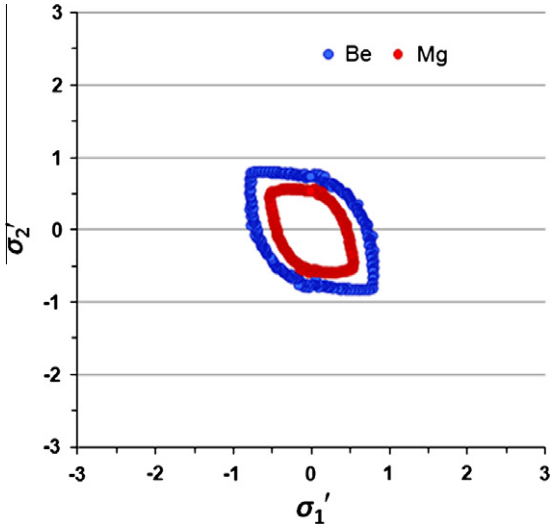

Fig. 4. The yield surfaces for case (a). σ_1' and σ_2' are the normalized resolved applied stresses on the basal $(0\,0\,0\,1)$ and prismatic $(0\,1\,\bar{1}\,0)$ planes, respectively. The junction is oriented along $[1\ -\sqrt{3}\ 0]$, equivalent to $[\bar{2}\,1\,1\,0]$ in the 4-index notation.

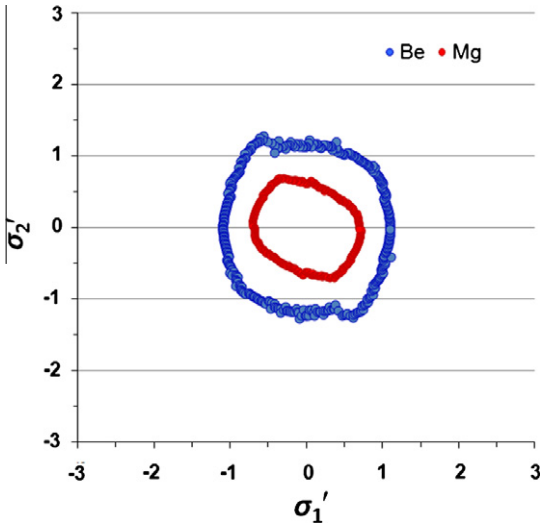

Fig. 5. The yield surfaces for case (b). σ_1' and σ_2' are the normalized resolved applied stresses on the type-II pyramidal $(\bar{2}\,1\,1\,2)$ and the prismatic $(0\,1\,\bar{1}\,0)$ planes, respectively. The junction is oriented along $[2\,\bar{1}\,\bar{1}\,3]$, equivalent to $[-1\ \sqrt{3}\ 2\frac{c}{a}]$ in the 4-index notation.

II-pyramidal slip planes [44]. In Grinberg et al.'s [44] work, it was found that dislocations of this type in Mg prefer to align along the $\langle 1\,\bar{1}\,0\,0\rangle$ direction.

3.2. Junction unzipping and yield surfaces

As shown in the linear dependence of the critical stress on μ in Eq. (2), the computed critical breaking stresses of junctions in Be should be one order of magnitude greater (in MPa) than in Mg. The relative strengths of junctions are compared via their yield surface plots. We use the

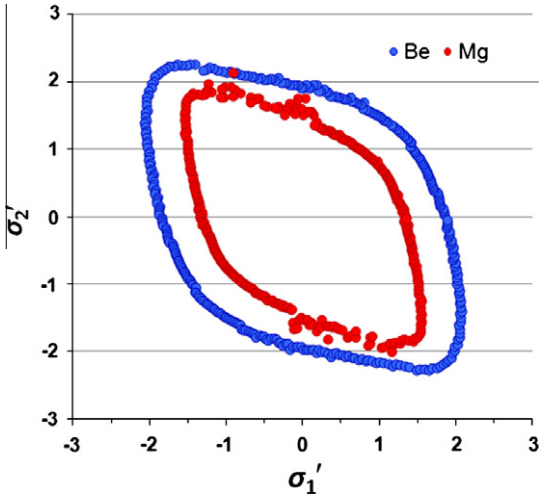

Fig. 6. The yield surfaces for case (c). The σ_1' and σ_2' are the normalized resolved applied stresses on the type-II pyramidal $(\bar{2}\,1\,1\,2)$ and the prismatic $(0\,1\,\bar{1}\,0)$ planes, respectively. The junction is oriented along $[2\,\bar{1}\,\bar{1}\,3]$, equivalent to $[-1\ \sqrt{3}\ 2\frac{c}{a}]$ in the 4-index notation.

normalized stress pairs of $(\sigma_{1,c}', \sigma_{2,c}')$ for the axes. These values are obtained by scaling the critical resolved stresses $(\sigma_{1,c}, \sigma_{2,c})$ using the following normalization factor

$$\sigma_{i,c} = \sigma_{i,c}' \left[\frac{\mu a}{L(1-\nu)} \ln\left(\frac{R}{r_o}\right) \right] \tag{9}$$

where the slip plane index is $i = 1, 2$, a is the lattice spacing, and L is the initial length of the intersecting dislocations. Here, the term "a" is in the numerator because L is in the unit of a, so that the normalized critical stresses $\sigma_{i,c}'$ are dimensionless. Figs. 4–6 depict the resultant yield surfaces for the junctions studied in this work.

The yield surfaces in all cases show a remarkable symmetry, which is anticipated because of the symmetric initial equilibrium junction with respect to a center line perpendicular to the junction, as described in Section 3.1. In the DDD simulations, such symmetry was checked by running all points for a complete envelope of yield surface. Earlier studies on the formation and destruction of binary junctions in fcc crystals using analytical models also attributed the symmetry of yield surfaces to the symmetry of junction triple nodes [11,19]. The appearance of this trend in hcp crystals suggests that these symmetries are independent of crystallographic structure. The shape of yield surfaces are along a straight line that represents the major axis of the elongated shapes, $\sigma_2 = m\sigma_1$, where m is the slope of that line. The positive or negative sign of m depends on the choice of slip planes used to create the junction and the consequence that choice has on the orthogonal Schmidt tensor $\boldsymbol{S}$. The symmetry and elongation also result from the dependence of critical breaking stresses on the sign of trial σ_1 and σ_2. The uniformity upon scaling with Eq. (9) reaffirms the sensitivity to the elastic constants of the material in light of the one order of magnitude difference in their elastic moduli and the difference in the Poisson's ratio.

The inclination of yield surfaces does not vary significantly in Figs. 4–6. The junction unzipping mechanism is sensitive to the Burgers vector of each dislocation. For the basal/prismatic junction in case (a), the $\langle a\rangle$-type Burgers vector on the prismatic plane is in the same direction as the junction, as indicated in Fig. 1. Therefore, the arms on the prismatic plane bow out in favor of junction destruction, resulting in smaller yield surfaces. Junction destruction, therefore, may be resisted or expedited by careful choices of interacting Burgers vectors. The role of Burgers vectors is more complex in the type-II pyramidal/prismatic junction. As evident in Tables 1 and 2, using $\frac{1}{3}[\bar{2}\,1\,1\,0]$, a pure $\langle a\rangle$ type, as the Burgers vector for the prismatic plane makes the junction a mixed dislocation for case (b). However, by changing the Burgers vector to $[0\,0\,0\,\bar{1}]$, a pure $\langle c\rangle$ type, the junction for case (c) is a pure edge due to its pure $\langle a\rangle$-type resultant Burgers vectors.

The elongated yield surface may also be related to the orthogonal Schmidt tensors $\boldsymbol{S}$, which are used for the calculation of trial applied stress $\boldsymbol{\sigma}$, although it is difficult to isolate their influences from those of the Burgers vectors. It is noted that the ratio of the major axis of yield surface to its minor axis is generally consistent with the ratio between the magnitude of $\boldsymbol{S}_2 + \mathrm{m}\boldsymbol{S}_1$ or $\boldsymbol{S}_2 - \mathrm{m}\boldsymbol{S}_1$ to those of $\boldsymbol{S}_1$ and $\boldsymbol{S}_2$ for all cases except case (b), which has relatively rounded yield surfaces. The ratios are ~1.5–1.7 for case (a) and ~1.6 for case (c). The results indicate that junctions with a greater edge component, such as in cases (a) and (c), are more likely to have an elongated yield surface than junctions with a greater screw component, such as in case (b). The junctions in case (b) are mixed dislocations with a stronger screw character. Capolungo [22] performed DDD simulations for junctions in Mg that yielded similar observations. Small differences from the present results may be explained by the difference in the normalization factor used.

The size of the yield surfaces evidently depends on the elastic constants because of their involvement, namely the ratio of $\mu/(1-\nu)$, in the normalization factor, as shown in Eq. (9). After normalization, the one-order difference in the magnitude of critical unzipping stresses between Be and Mg can be largely eliminated. However, the differences in sizes between these two materials are then dominated by the Poisson's ratio term $(1-\nu)$, for which the ratio between Mg and Be is 0.71, making the yield surfaces for Be larger than those for Mg in all cases. From the DDD-obtained yield surfaces, interacting Burgers vector pairs both of $\langle a\rangle$ type would result in smaller yield surfaces, resembling those in fcc crystals [11], as in the present case (a). This can be attributed to the fact that all the involved Burgers vectors are $\langle a\rangle$ type, which is the shortest lattice vector on the basal plane, the only close-packed slip plane in hcp crystals resembling the $\langle 1\,1\,1\rangle$ slip planes in fcc crystals. Moreover, the basal/prismatic junction in case (a) is a mixed dislocation with a 60° orientation to its Burgers vector, a similar geometry to those in fcc crystals. This may explain why the yield surfaces in case (a) appear to resemble those reported for fcc crystals, except that those in fcc crystals elongate along the positive diagonal direction.

However, Burgers vector pairs of different types involving either a type $\langle a\rangle$ or a type $\langle c\rangle$ interacting with a type $\langle a+c\rangle$ would make the yield surfaces differ from fcc crystals, such as in cases (b) and (c). This can be attributed to the different magnitudes of interacting Burgers vector pairs. The sensitivity to the chosen Burgers vectors indicates the sensitivity of yield surfaces on crystal type. For both Be and Mg, the junctions in case (c) exhibit significantly larger yield surfaces than cases (a) and (b). This can also be attributed to the ~80% reduction in the total dislocation energy via junction formation for case (c), in comparison with, at most, 50% reduction for the junctions formed in other cases. These findings also indicate the possible extension from fcc crystals to hcp crystals for the correlations between the total energy reduction due to the formation of a binary junction and its strength. Using yield surfaces calculated by the line tension model, Dupuy and Fivel [11] presented a direct comparison among different junctions in fcc crystals, including the Hirth lock, glissile junction and the Lomer–Cottrell lock. Their results also indicated the consistent trends of an increasing total energy reduction resulting in a stronger junction.

3.3. The effect of dislocation length on critical unzipping stresses

As predicted by the line tension approximation, the critical stress needed to break a junction should be proportional to $\ln(L)/L$, where L is the initial dislocation length prior to junction formation [9,45]. This relation has also been validated previously by MD and DDD simulations for junctions in fcc crystals [14,19]. To test this trend and

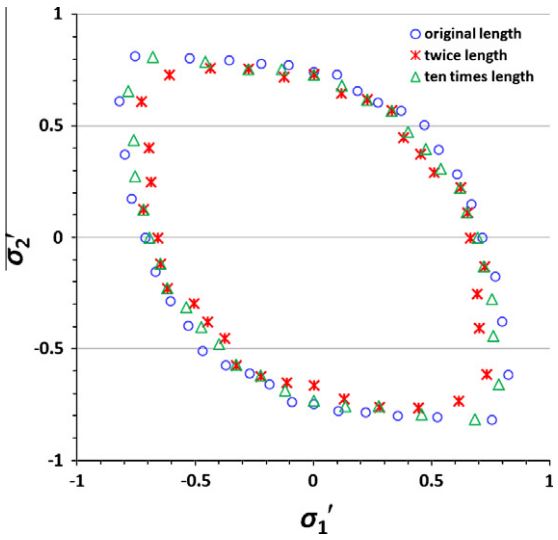

Fig. 7. The yield surfaces for the junction in Be in case (a) with varying initial dislocation lengths. The data points shown for the original initial dislocation length are identical to those for Be in Fig. 4. The junction is oriented along $[1\ -\sqrt{3}\ 0]$, equivalent to $[\bar{2}\,1\,1\,0]$ in the 4-index notation.

use the basal/prismatic junction in Be as an example, the initial dislocation lengths are varied two and ten times the original length of 40,000a. The magnitude of the critical resolved stresses reduce accordingly with increasing dislocation length. Fig. 7 displays the yield surfaces after scaling by $\ln(L)/L$. Thus, the effect of initial dislocation length is accounted for through the scaling.

4. Conclusions

We have studied the formation and dissolution mechanisms of non-coplanar dislocation junctions in Be and Mg via DDD simulations, with a special focus on examining the influences of material elasticity and active Burgers vectors on the junction strength. A complete junction dissolution appears to be most sensitive to the elastic properties. The critical stresses required to break junctions are shown by computing the loci of points that form yield surfaces. Separate yield surfaces are generated for both materials in alternate junction configurations, using different sets of interacting Burgers vectors. Upon normalization to account for differing elastic properties and initial dislocation lengths, all yield surfaces are symmetric, but change their sizes or shapes with the Burgers vectors involved. The significantly smaller yield surfaces obtained with both interacting Burgers vector pairs of type $\langle a \rangle$ resemble the shape of those in fcc crystals. However, the yield surfaces change either shape or size when the Burgers vectors involved are of different types with different magnitudes. It was also found that junctions possessing Burgers vectors with greater edge character show elongated and reclined yield surfaces, while those with a more screw character exhibit more rounded yield surfaces. For all cases studied in this work, the yield surfaces for Be are larger than those for Mg. The larger sizes of yield surfaces for the type-II pyramidal/prismatic junctions formed using interacting $\langle a + c \rangle$- and $\langle c \rangle$-type Burgers vectors generally affirms that more energetically favorable junction formations lead to stronger resultant junctions. Furthermore, using a scaling factor to account for length effects, the yield surfaces can be shown to be independent of the initial simulated dislocation lengths.

Acknowledgements

This work was conducted through support from the Oak Ridge Affiliated Universities (ORAU) in Maryland under Contract No. W911QX-04-C-0129 at the US Army Research Laboratory, the Army Research Laboratory (ARL) Enterprise for Multiscale Research of Materials and the ARL Director's Research Initiative (DRI). Computing resources were provided by the Department of Defense (DoD) High Performance Supercomputing Resource Center (DSRC). This work was also performed under the auspices of the US Department of Energy by Lawrence Livermore National Laboratory under Contract No. DE-AC52-07NA27344. The authors gratefully appreciate many valuable discussions with colleagues at ARL, including Kenneth A. Jones, Jaroslaw Knap, Joshua Crone and Kenneth Leiter.

References

[1] Hirth JP, Lothe J. Theory of dislocations. 2nd ed. Malabar, FL: Krieger; 1982 [chapter 22].
[2] Weertman J, Weertman JR. Elementary dislocation theory. Oxford: Oxford University Press; 1992 [chapter 5].
[3] Hirth JP. J Appl Phys 1961;32:700.
[4] Devincre B, Kubin LP. Modelling Simul Mater Sci Eng 1994;2:559.
[5] Lee MG, Lim H, Adams BL, Hirth JP, Wagoner RH. Int J Plast 2010;26:925.
[6] Schoeck G, Frydman R. Phys Stat Sol (b) 1972;53:661.
[7] Madec R, Devincre B, Kubin LP, Hoc T, Rodney D. Science 2003;301:1879.
[8] Friedel J. Dislocations, international series of monographs in solid state physics: 3. Oxford: Pergamon Press; 1964.
[9] Bulatov VV, Abraham FF, Kubin LP, Devincre B, Yip S. Nature 1998;391:669.
[10] Bulatov VV, Hsiung LL, Tang M, Arsenlis A, Bartelt MC, Cai W, et al. Nature 2006;440:1174.
[11] Dupuy L, Fivel MC. Acta Mater 2002;50:4873.
[12] Zhou SJ, Preston DL, Lomdahl PS, Beazley DM. Science 1998;279:1525.
[13] Zhou SJ, Preston DL. Physica D 1999;133:498.
[14] Rodney D, Phillips R. Phys Rev Lett 1999;82:1704.
[15] Zbib HM, de la Rubia TD, Rhee M, Hirth JP. J Nucl Mater 2000;276:154.
[16] Madec R, Devincre B, Kubin LP. Comput Mater Sci 2002;23:219.
[17] Lee SW, Aubry S, Nix WD, Cai W. Modelling Simul Mater Sci Eng 2011;19:025002.
[18] Wickham LK, Schwarz KW, Stölken JS. Phys Rev Lett 1999;83:4574.
[19] Shenoy VB, Kukta RV, Phillips R. Phys Rev Lett 2000;84:1491.
[20] Motz C, Weygand D, Senger J, Gumbsch P. Acta Mater 2009;57:1744.
[21] Carrez P, Cordier P, Devincre B, Kubin LP. Mater Sci Eng A 2005;400–401:325.
[22] Capolungo L. Acta Mater 2011;59:2909.
[23] Monnet G, Devincre B, Kubin LP. Acta Mater 2004;52:4317.
[24] Yoo MH, Agnew SR, Morris JR, Ho KM. Mater Sci Eng A 2001;319–321:87.
[25] Kim DH, Ebrahimi F, Manuel MV, Tulenko JS, Phillpot SR. Mater Sci Eng A 2011;528:5411.
[26] Balogh L, Figueiredo RB, Ungár T, Langdon TG. Mater Sci Eng A 2010;528:533.
[27] Kuwano N, Tsuruda T, Kida Y, Miyake H, Hiramatsu K, Shibata T. Phys Stat Sol (c) 2003:2444.
[28] Bai J, Wang T, Parbrook PJ, Wang Q, Lee KB, Cullis AG. Appl Phys Lett 2007;91:131903.
[29] Wu XH, Fini P, Tarsa EJ, Heying B, Keller S, Mishra UK, et al. J Cryst Growth 1998;189–190:231.
[30] Newnham RE. Properties of materials: anisotropy, symmetry, structure. Oxford: Oxford University Press; 2005 [chapter 13].
[31] Hull D, Bacon DJ. Introduction to dislocations. 3rd ed. London: Butterworth-Heinenmann; 1984.
[32] Osipiyan YA, Smirnova IS. J Phys Chem Solids 1971;32:1521.
[33] Arsenlis A, Cai W, Tang M, Rhee M, Oppelstrup T, Hommes G, et al. Modelling Simul Mater Sci Eng 2007;15:553.
[34] Damiano VV. Trans Metall Soc AIME 1963;227:788.
[35] Zwillinger D. (Editor in Chief). CRC standard mathematical tables and formulae, 30th ed. Boca Raton, FL: CRC Press; 2011 [chapter 2].
[36] Capolungo L, Beyerlein IJ, Wang ZQ. Modelling Simul Mater Sci Eng 2010;18:085002.
[37] Wu C, Aubry S, Chung PW, Arsenlis A. Mater Res Soc Symp Proc 2012;1424.

[38] Tadmor EB, Miller RE, Elliott RS. Continuum mechanics and thermodynamics: from fundamental concepts to governing equations. Cambridge: Cambridge University Press; 2012 [chapter 6].
[39] Martinez E, Marian J, Arsenlis A, Victoria M, Perlado JM. J Mech Phys Sol 2008;56:869.
[40] deWit G, Koehler JS. Phys Rev 1959;116:1113.
[41] Frank FC, Read WT. Phys Rev 1950;79:722.
[42] Dash WC. J Appl Phys 1956;27:1193.
[43] Hirth JP, Lothe J. Theory of dislocations. 2nd ed. Malabar, FL: Krieger; 1982 [chapter 5, p. 123].
[44] Grinberg BA, Ivanov MA, Antonova OV, Vlasova AM, Kruglikov NA, Plotnikov AV. Russ Phys J 2011;54:906.
[45] Hirth JP, Lothe J. Theory of dislocations. 2nd ed. Malabar, FL: Krieger; 1982 [chapter 3, p. 91].

NO. OF COPIES	ORGANIZATION
1 (PDF)	DEFENSE TECHNICAL INFORMATION CTR DTIC OCA
2 (PDF)	DIRECTOR US ARMY RESEARCH LAB RDRL CIO LL IMAL HRA MAIL & RECORDS MGMT
1 (PDF)	GOVT PRINTG OFC A MALHOTRA
3 (PDF)	DIR USARL RDRL CIH C LB MUNDAY M SCHEPLENG C-C WU
1 (PDF)	UNIV MARYLAND PW CHUNG

INTENTIONALLY LEFT BLANK.